Iron to catalyze ammonia synthesis at low temperature

Michikazu Hara (mhara@msl.titech.ac.jp)
Tokyo Institute of Technology https://orcid.org/0000-0003-3450-5704
Masashi Hattori
Tokyo Institute of Technology https://orcid.org/0000-0002-0644-5137
Natsuo Okuyama
Tokyo Institute of Technology
Hiyori Kurosawa
Tokyo Institute of Technology

Physical Sciences - Article

Keywords:

Posted Date: April 12th, 2022

DOI: https://doi.org/10.21203/rs.3.rs-1426351/v1

Abstract

Ammonia is used to provide food for over 5 billion people; however, it is currently required to be produced without the use of fossil fuels to reduce global CO2 emissions by 3% or more. To significantly decrease the energy consumed to produce ammonia from H2 and N2 with heterogeneous catalyst by the Haber-Bosch (HB) process, both H2 production from water and the HB process could be driven with only renewable electricity toward ammonia production without CO2 emissions. It is thus indispensable to devise heterogeneous catalysts for the synthesis of ammonia below 100–150 °C to minimize the energy consumption of the process. Furthermore, the desired catalyst should be produced from ubiquitous and abundant resources on a large scale to maintain ammonia production that would reach 170 million tons per year. Here we report metallic iron as a catalyst for ammonia synthesis at 100 °C in combination with an electron-donating material as a new approach. The iron catalyst revealed that iron can exhibit a few hundred to several thousand times higher efficiency (turnover frequency) for ammonia synthesis than other transition metals used in highly active catalysts because of the intrinsic nature of iron to desorb adsorbed hydrogen atoms as hydrogen molecules at low temperature.

Full Text

Ammonia is used to provide food for over 5 billion people; however, it is currently required to be produced without the use of fossil fuels to reduce global CO_2 emissions by 3% or more.[1,2] To significantly decrease the energy consumed to produce ammonia from H_2 and N_2 with heterogeneous catalyst by the Haber-Bosch (HB) process, both H_2 production from water and the HB process could be driven with only renewable electricity toward ammonia production without CO_2 emissions.[3-5] It is thus indispensable to devise heterogeneous catalysts for the synthesis of ammonia below 100–150 °C to minimize the energy consumption of the process. Furthermore, the desired catalyst should be produced from ubiquitous and abundant resources on a large scale to maintain ammonia production that would reach 170 million tons per year. Here we report metallic iron as a catalyst for ammonia synthesis at 100 °C in combination with an electron-donating material as a new approach. The iron catalyst revealed that iron can exhibit a few hundred to several thousand times higher efficiency (turnover frequency) for ammonia synthesis than other transition metals used in highly active catalysts because of the intrinsic nature of iron to desorb adsorbed hydrogen atoms as hydrogen molecules at low temperature.

Driving both hydrogen production by water electrolysis and the HB process with only renewable electricity, such as wind power generation, is a promising way to produce ammonia without CO_2 emissions. Nevertheless, it is significantly inferior to the conventional ammonia production using H_2 obtained from fossil fuels in terms of energy consumption because the HB process operates at high temperature and pressure, and is driven only by electricity (Fig. 1a).[3-6] Any catalyst that can allow the operating temperature to be decreased below 100–150 °C would reduce the energy consumed for the HB process by 70 to 80% (Fig. 1b) and decrease the difference in energy consumption between conventional and CO_2-free methods (Fig. 1a). The issue with CO_2-free ammonia production has been also a significant

issue in the HB process for over 100 years and has pushed recent research toward low temperature ammonia synthesis. Most of the recently reported highly active catalysts use Ru, Co, and Ni as reaction sites because these can be easily deposited on supports as highly dispersed metal nanoparticles that exhibit high catalytic performance.[7-11] While we have also discovered a unique Ru-based heterogeneous catalyst to synthesize ammonia from H_2 and N_2, even below 100 °C,[12] we have questioned whether catalysts that use these transition metals have significant potential to increase the catalytic activity at the desired reaction temperature of ≤100–150 °C from the perspective of the H_2 adsorption/desorption equilibrium. The dissociative adsorption of H_2 and H_2 desorption from the resulting adsorbed H atoms (H adatoms) are in an equilibrium on all transition metal surfaces in the synthesis of ammonia as well as N_2 adsorption/desorption. It is well-known for Ru catalysts that adsorption of H adatoms onto the transition metal surfaces is preferential, so that the H_2 adsorption/desorption equilibrium shifts toward H_2 adsorption, which decreases ammonia formation by the decrease in adsorption sites for N adatoms (Fig. 1c).[13,14] Such “hydrogen-poisoning” can affect all transition metals used in the synthesis of ammonia. Attributing hydrogen-poisoning to the bond strength between H adatoms and the surface transition metal atoms, it is anticipated that this effect is enhanced with a decrease in ammonia synthesis temperature because a larger amount of H adatoms would be more tightly adsorbed on the transition metal surfaces with a decrease in temperature (Fig. 1c). As a result, hydrogen-poisoning would be a major obstacle to the desirable low temperature ammonia synthesis over catalysts that employ transition metals as the active sites. In the present study, we have again focused on iron used as the reaction sites since the beginning of the HB process. Iron has been regarded as a classical transition metal that is inferior to other transition metals for ammonia synthesis. Several catalysts that use other transition metals exhibit much higher catalytic performance for ammonia synthesis than iron-based catalysts used in the present HB process.[8,12] In addition, no effective ways to use iron for ammonia synthesis at low temperatures as low as 100 °C have been found to date. On the other hand, ammonia synthesis over iron-based catalysts has not been reported to be strongly influenced by hydrogen-poisoning. This suggests that the H_2 adsorption/desorption equilibrium on iron surfaces is shifted more toward H_2 desorption, and thus a decrease in the H adatom concentration than with other transition metals. Therefore, iron may be used for ammonia synthesis while preventing hydrogen-poisoning, even at low temperatures, if iron can be combined with an appropriate promoter in an appropriate manner. The use of ubiquitous, abundant, and inexpensive iron is also a significant advantage with respect to the environment and economy.

In several tested catalyst designs, only a new type of catalyst design, metallic iron particles loaded with a mixture of BaO and BaH_2 (BaH_2-BaO/Fe), was effective for low temperature ammonia synthesis. Conventional supported iron catalysts, where iron nanoparticles are deposited on support particles with electron-donating capability, could not act as catalysts for ammonia synthesis below 200 °C. BaH_2-BaO/Fe was readily prepared by heating $Ba(NO_3)_2$-impregnated Fe_2O_3 particles (20–40 nm) with CaH_2 particles at 300 °C in a flow of H_2. Figs. 2a and b for the resulting material display that Ba species composed of BaO and BaH_2 are segregated on metallic iron particles (>10–30 nm) in contact with CaH_2. Therefore, the preparation procedure readily leads to iron particles loaded with a mixture of BaO and

BaH_2, as schematically shown in Fig. 2c. We reported that BaH_2 can exhibit strong electron-donating capability in BaH_2-BaO with deposited Ru nanoparticles (Ru/BaH_2-BaO).[15] A part of the BaH_2 in BaH_2-BaO releases H atoms from H^- anions as H_2 molecules through transition metal surfaces, so that electrons remain in BaH_2 to release H atoms ($BaH_2 \leftrightarrow Ba^{2+}H^-_{(2-x)}e^-_x + xH \leftrightarrow Ba^{2+}H^-_{(2-x)}e^-_x + x/2H_2$). The strong electron donation from the BaH_2 species ($Ba^{2+}H^-_{(2-x)}e^-_x$) to N_2 adsorbed on the transition metal surfaces facilitates N_2 cleavage. The temperature at which H_2 begins to desorb corresponds to the lowest catalyst working temperature. It was confirmed that ammonia synthesis over Ru nanoparticles deposited on $Ca^{2+}F^-H^-$ (Ru/CaFH) also proceeded at 50 °C in a similar manner to that over Ru/BaH_2-BaO.[12] H_2-temperature programmed desorption (TPD) revealed that BaH_2-BaO/Fe desorbs H_2 above ca. 100 °C (Fig. 2d). As a result, BaH_2 species ($Ba^{2+}H^-_{(2-x)}e^-_x$) with strong electron-donating capability are formed that can donate electrons to metallic Fe at this temperature. The electron-donating capability of $Ba^{2+}H^-_{(2-x)}e^-_x$ was estimated by density functional theory (DFT) calculations. The work functions for the (001) surfaces of $Ba^{2+}H^-_2$ and $Ba^{2+}H^-_{(2-x)}e^-_x$ (x=1/9, $Ba^{2+}H^-_{(2-1/9)}e^-_{1/9}$) were estimated to be Φ=4.2 and 2.6 eV, respectively, by DFT computation (Extended Data Fig. 1). Thus, the removal of H atoms from BaH_2 can form BaH_2 species with high electron-donating capability, comparable to those of metallic K and Na (Φ=2.3 and 2.4 eV, respectively).

Fig. 3a shows the catalytic performance for ammonia synthesis (100-200 °C, 0.9 MPa) over BaH_2-BaO/Fe and Ru/BaH_2-BaO. In Ru/BaH_2-BaO, Ru metal nanoparticles (2-4 nm) are deposited on BaH_2-BaO phase formed on CaH_2 large particles (several 30 μm).[15] The results for a commercial promoted iron catalyst (promoted-Fe) that consists of Fe, K_2O, Al_2O_3 and CaO, MgO loaded with Ru nanoparticles and Cs oxide species (Cs-Ru/MgO), and Ru-nanoparticles deposited on $[Ca_{24}Al_{28}O_{64}]^{4+}(e^-)_4$ (Ru/C12A7:e^-) as benchmark catalysts are also shown. Extended Data Table 1 summarizes the ammonia synthesis activities of the tested materials and representative catalysts with physicochemical information, including metal particle sizes and surface areas. The promoted-Fe catalyst, which was first found by Haber, Bosch and Mittasch more than 100 years ago and has been improved since then, is not inferior to most of the recently reported catalysts; only a handful of recent catalysts surpass the iron catalyst in terms of ammonia synthesis activity (Extended Data Table 1).[8,15-17] Nevertheless, promoted-Fe could not form ammonia below 200 °C. Cs-Ru/MgO and Ru/C12A7:e^- also did not work for ammonia synthesis below 200 °C. In contrast, BaH_2-BaO/Fe first revealed that iron can catalyze ammonia synthesis at 100 °C. The rate of ammonia formation increased with the reaction temperature. Ammonia formation proceeded over BaH_2-BaO/Fe without a significant decrease in activity for over 100 h (Fig. 3b). Taking into account the number of zero-valent Fe atoms on the iron surface of the catalyst, the reaction for 100 h was estimated to give a turnover number of ca. 600 thousand (6.12×10^5); BaH_2-BaO/Fe with a new type of catalyst structure acts as a stable catalyst.

Ru/BaH_2-BaO was inferior to BaH_2-BaO/Fe in ammonia formation rate below 200 °C, even although both catalysts use the same electron-donating material. The difference is further emphasized with respect to

the ammonia formation turnover for the surface zero-valent Fe and Ru atoms (turnover frequency; TOF). In Fig. 3a, BaH_2-BaO/Fe exhibits TOFs that are several thousand times higher than Ru/BaH_2-BaO. In heterogeneous catalysts that adopt Ru, Co and Ni as the active sites for ammonia synthesis, the maximum TOF is at most less than 0.17 s^{-1}, even at 400 °C (Extended Data Table 2).[11] However, the TOF of the iron catalyst was 0.23 s^{-1} at 100 °C and reached 12.3 s^{-1} at 300 °C. To understand the difference in catalysis between Fe and Ru promoted by the same electron-donating material, the correlation of ammonia formation rate with total pressure and the reaction orders in the rate equation on BaH_2-BaO/Fe and Ru/BaH_2-BaO were measured at 200 °C and are summarized in Fig. 3c. The ammonia formation rate for Ru/BaH_2-BaO is independent of the pressure or gradually decreased with the pressure, and the reaction order for H_2 showed a negative value of -0.79; an increase in reactant concentration cannot lead to an increase in product formation. These results are inconsistent with kinetics theory and are clearly due to hydrogen-poisoning,[13,14] where the Ru surface on Ru/BaH_2-BaO is severely poisoned by H adatoms and cannot exhibit satisfactory catalytic performance for ammonia formation as shown in Fig. 1c. Such a hydrogen-poisoned Ru surface would not show a high TOF. On the other hand, the rate of ammonia formation increased in proportion to the pressure over BaH_2-BaO/Fe to show a positive value of +0.47 as the reaction order for H_2. As a result, the iron catalyst is not strongly affected by hydrogen poisoning, even at 200 °C, which results in a much higher TOF than those of Ru-based catalysts. One possible explanation for hydrogen-poisoning due to the H_2 adsorption/desorption equilibrium on transition metals is the density and strength of the bonds between H adatoms and surface transition metal atoms. Because a larger amount of H adatoms is expected to be more tightly adsorbed on transition metal surfaces with a decrease in temperature, we may clarify the effect of hydrogen-poisoning by observing H_2 desorption from BaH_2-BaO/Fe and Ru/BaH_2-BaO at low temperature. Fig. 3d shows molecular deuterium (D_2)-TPD measurements for both the catalysts. The desorption of D adatoms due to gas phase D_2 can be distinguished from the desorption of H adatoms originated from H^- anions in BaH_2-BaO through transition metals by the use of D_2-TPD. Most D adatoms desorbed as D_2 from the iron catalyst at 40–100 °C. It was confirmed that D_2 desorption from the iron catalyst is consistent with H_2 desorption from a single crystal iron surface.[19] This means that the iron surface provides sufficient adsorption sites for N_2 and N adatoms without a strong influence of hydrogen-poisoning under ammonia synthesis conditions above 100 °C. In the case of Ru/BaH_2-BaO, a large D_2 desorption peak was observed at 125–225 °C; Ru binds to H adatoms more tightly than iron, and these H adatoms can cause hydrogen-poisoning on Ru over a broad temperature range. Co and Ni surfaces have also been found to strongly adsorb H adatoms that are desorbed as H_2 at > 150–200 °C as with Ru.[20-22] These results imply that many transition metals used to synthesize ammonia can be significantly affected by hydrogen-poisoning at low temperatures and iron is an exceptional transition metal that prevents hydrogen-poisoning. The difference in hydrogen-poisoning may be expressed as the difference in TOF among BaH_2-BaO/Fe and the other transition metal-based catalysts.

Ammonia synthesis over the iron catalyst was further studied to understand the reaction mechanism. The energy diagram obtained from the heat of dissociative adsorption of N_2 ($\Delta H\ N_2 \rightarrow 2N$), the apparent activation energies for ammonia synthesis (Ea NH_3) and N_2 desorption from N adatoms (Ea $2N \rightarrow N_2$) on BaH_2-BaO/Fe is shown in Fig. 4a with the details. From these thermodynamic data, the activation energy for N_2 cleavage (Ea $N_2 \rightarrow 2N$) on BaH_2-BaO/Fe was estimated to be below 16 kJ mol^{-1}. This value is too small compared with the apparent activation energy (Ea NH_3=40 kJ mol^{-1}) for ammonia synthesis over BaH_2-BaO/Fe if we regard Ea $N_2 \rightarrow 2N$ as the apparent activation energy, *i.e.,* the activation energy for the rate-determining step (Fig. 4a-A). Consequently, it is consistent that the rate-determining step of ammonia synthesis on BaH_2-BaO/Fe is not N_2 cleavage, but the formation of subsequent N-Hn species such as NH, NH_2 and NH_3 (Fig. 4a-B). In ammonia formation composed of N_2 decomposition and N-Hn species formation, the former step has been regarded as the rate-determining step in most catalysts.[23] To decrease the activation energy for the former below those of the latter by weakening strong N≡N triple bonds requires electron donation from the electron-donating materials to the antibonding π* orbitals of adsorbed N_2 via transition metal d-orbitals to be boosted. In the Fourier transform infrared (FT-IR) spectrum (Fig. 4b) for N_2 adsorbed on Ru/C12A7:e^-, the νN_2 band appeared at 2100-2200 cm^{-1}, lower than that of N_2 (2150-2250 cm^{-1}) adsorbed on Ru nanoparticles-deposited Al_2O_3 support (Ru/Al_2O_3) because C12A7:e^- (work function Φ=2.1 eV) has a stronger electron-donating capability than Al_2O_3 (Φ=4.7 eV).[7] Ru/C12A7:e^- is an exceptional catalyst to shift the rate-determining step from N_2 cleavage to N-H species formation by the strong electron-donating capability of C12A7:e^- as with BaH_2-BaO/Fe.[24] Fig. 4b also displays that νN_2 for N_2-adsorbed BaH_2-BaO/Fe is observed as a broad band in the range of 2000-2175 cm^{-1}, which is lower than of Ru/C12A7:e^-, and disappears after the removal of N adatoms by evacuation. Thus, the iron catalyst is more electron-donating than Ru/C12A7:e^-, which reduces the activation energy for N_2 decomposition below those for the formation of N-Hn species.

As a summary of these results, the mechanism postulated for ammonia synthesis over BaH_2-BaO/Fe is shown schematically in Fig. 4c. The shift of the H_2 adsorption/desorption equilibrium toward H_2 desorption on the iron surfaces does not only give the strong electron-donating capability to BaH_2-BaO, but also provides sufficient adsorption sites for N_2 molecules on iron surface. This results in a high TOF for ammonia synthesis over the iron catalyst to prevent hydrogen-poisoning. Therefore, Iron, which was first found to catalyze ammonia formation at high temperature by Haber, Bosch and Mittasch over a century ago, may be also effective for low temperature ammonia synthesis.

Online content

Any methods, additional references, Nature Research reporting summaries, extended data, acknowledgements and peer review information; details of author contributions are available at XXXX

References

1. Song, P., Kang, L., Wang, H., Guo, R. & Wang, R. Nitrogen (N), phosphorus (P)-codoped porous carbon as a metal-free electrocatalyst for N_2 reduction under ambient conditions. *ACS Appl. Mater. Interfaces* **11**, 12408–12414 (2019).
2. Hara, M., Kitano, M. & Kamata, K. Ru-loaded C12A7:e^- electride as a catalyst for ammonia synthesis. *ACS Catal.* **7**, 2312–2324 (2017).
3. Smith, C., Hill, A. K. & Torrente-Murciano, L. Current and future role of Haber-Bosch ammonia in a carbon-free energy landscape. *Energy Environ. Sci.* **13**, 331–344 (2020).
4. Rouwenhorst, K. H. R., Van der Ham, A. G. J., Mul, G. & Kersten, S. R. A. Islanded ammonia power systems: Technology review & conceptual process design. *Renew. Sustain. Energy Rev.* **114**, 109339 (2019).
5. Ghavam, S., Vahdati, M., Wilson, I. A. G. & Styring, P. Sustainable ammonia production processes. *Front. Energy Res.* **9**, 580808 (2021).
6. Tallaksen, J. & Reese, M. Ammonia production using wind energy. http://nh3fuelassociation.org/2013/08/28/ammonia-production-using-wind-energy (2013).
7. Kitano, M. et al. Ammonia synthesis using a stable electride as an electron donor and reversible hydrogen store. *Nat. Chem.* **4**, 934–940 (2012).
8. Kitano, M. et al. Self-organized ruthenium-barium core-shell nanoparticles on a mesoporous calcium amide matrix for efficient low-temperature ammonia synthesis. *Angew. Chem. Int. Ed.* **130**, 2678–2682 (2018).
9. Wang, P. K. et al. Breaking scaling relations to achieve low-temperature ammonia synthesis through LiH-mediated nitrogen transfer and hydrogenation. *Nat. Chem.* **9**, 64–70 (2017).
10. Gao, W. B. et al. Barium hydride-mediated nitrogen transfer and hydrogenation for ammonia synthesis: a case study of cobalt. *ACS Catal.* **7**, 3654–3661 (2017).
11. Ye, T-N. et al. Vacancy-enabled N_2 actinvation for ammonia synthesis on an Ni-loaded catalyst. *Nature* **583**, 391–407 (2020).
12. Hattori, M., Iijima, S., Nakao, T., Hosono, H. & Hara, M. Solid solution for catalytic ammonia synthesis from nitrogen and hydrogen gases at 50 °C. *Nat. Commun.* **11**, 2001 (2020).
13. Rosowski, F., Hornung, A., Hinrichsen, O., Herein, D., Muhler, M. & Ertl, G. Ruthenium catalysts for ammonia synthesis at high pressures: Preparation, characterization, and power-law kinetics. *Appl. Catal. A* **151**, 443–460 (1997).
14. Siporin, S. E. & Davis, R. J. Use of kinetic models to explore the role of base promoters on Ru/MgO ammonia synthesis catalysts. *J. Catal.* **225**, 359–368 (2004).
15. Hattori, M. et al. Enhanced catalytic ammonia synthesis with transformed BaO. *ACS Catal.* **8**, 10977–10984 (2018).
16. Ogura, Y. et al. Efficient ammonia synthesis over a Ru/$La_{0.5}Ce_{0.5}O_{1.75}$ catalyst pre-reduced at high temperature. *Chem. Sci.* **9**, 2230–2237 (2018).

17. Ogura, Y. et al. Ru/$La_{0.5}Pr_{0.5}O_{1.75}$ catalyst for low-temperature ammonia synthesis. *ACS Sustainable Chem. Eng.* **6**, 17258–17266 (2018).
18. Ashida, Y., Arashiba, K., Nakajima, K. & Nishibayashi, Y. Molybdenum-catalysed ammonia production with samarium diiodide and alchols or water. *Nature* **568**, 536–551 (2019).
19. Bozso, F., Ertl, G., Grunze, M. & Weiss, M. Chemisorption of hydrogen on iron surfaces. *Appl. Surf. Sci.* **1**, 103–119 (1977).
20. Xue, X. et al. Double-active site synergistic catalysis in Ru-TiO_2 toward benzene hydrogenation to cyclohexene with largely enhanced selectivity. *Catal. Sci. Technol.* **7**, 650–657 (2017).
21. Huesges, Z. & Christmann, K. Interaction of hydrogen with a cobalt(0001) surface. *Z. Phys. Chem.* **227**, 881–889 (2013).
22. Znak, L. & Zielinski, J. Effects of support on hydrogen adsorption/desorption on nickel. *Appl. Catal. A.* **334**, 268–276 (2008).
23. Vojvodic, A. et al. Exploring the limits: A low-pressure, low-temperature Haber-Bosch process. *Chem. Phys. Lett.* **598**, 108–112 (2014).
24. Kitano, M. et al. Electride support boosts nitrogen dissociation over ruthenium catalyst and shifts the bottleneck in ammonia synthesis. *Nat. Commun.* **6**, 6731 (2015).
25. Hinrichsen, O., Rosowski, F., Hornung, A., Muhler, M. & Ertl, G. The kinetics of ammonia synthesis over Ru-based catalysts.1. The dissociative chemisorption and associative desorption of N_2. *J. Catal.* **165**, 33–44 (1997).
26. Hayashi, F. et al. Ammonia decomposition by ruthenium nanoparticles loaded on inorganic electride C12A7:e^-. *Chem. Sci.* **4**, 3124–3130 (2013).
27. Yeo, B. C. et al. Electronic structural origin of the catalytic activity trend of transition metals for electrochemical nitrogen reduction. *J. Phys. Chem. C* **123**, 31026–31031 (2019).
28. Kuganathan, N., Hosono, H., Shluger, A. L. & Sushko, P. V. Enhanced N_2 dissociation on Ru-loaded inorganic electride. *J. Am. Chem. Soc.* **136**, 2216–2219 (2014).

Methods

Catalyst preparation.

Iron particles loaded with and without BaH_2-BaO (BaH_2-BaO/Fe, Fe particles). BaO-BaH_2/Fe and Fe particles. 7.0 g of $Fe(NO_3)_3 \cdot 9H_2O$ (Kanto Chemical) was dissolved in 30 mL of distilled water. Water was removed from the solution by a rotary evaporator at 70 °C, and the remaining red solid was heated at 300 °C for 10 h in air to yield α-Fe_2O_3 powder. After 0.20 g of α-Fe_2O_3 and 0.052 g of $Ba(NO_3)_2$ (High Purity Chemicals) were stirred in 10 mL of distilled water for 30 min, water was evaporated at 70 °C. 0.023 g of the resultant $Ba(NO_3)_2$-impregnated α-Fe_2O_3 and 0.077 g of CaH_2 were mixed in an alumina mortar inside an Ar-filled glovebox. The atomic ratio of Fe:Ba:Ca in the mixture was 12.5:1:100. The mixture was heated in a flow of H_2 (45 mL min^{-1}) at 300 °C for 2h, which resulted in BaO-BaH_2/Fe. Fe particles, *i.e.*, metallic

iron particles without BaO-BaH_2, were obtained by heating 0.019 g of α-Fe_2O_3 with 0.081 g of CaH_2 in a flow of H_2 (45 mL min^{-1}) at 300 °C for 2h.

Ru or iron nanoparticles deposited on BaH_2-BaO (Ru/BaH_2-BaO). According to previous reports,[15] Ru/BaH_2-BaO was prepared by heating a mixture of 3 mol% BaO (Kojundo Chemical) and 97 mol% CaH_2 with $Ru(acac)_3$ corresponding to 10 wt% Ru or Fe at 260 °C in a flow of H_2 (2.5 mL min^{-1}). After 2 h, the samples were heated at 340 °C for 10 h in a H_2 flow. In the resulting materials, transition metal nanoparticles are deposited on BaH_2-BaO phase formed on CaH_2 large particles (several 30 μm).[15]

Evaluation of catalytic performance. Ammonia synthesis over each catalyst was examined in a stainless steel fixed bed reactor (catalyst; 0.1 g) at 300 °C under a flow of N_2–H_2 (N_2:H_2 = 1:3, 60 mL min^{-1}, weight hourly space velocity (WHSV): 36000 mL g cat^{-1} h^{-1}) at 0.9 MPa. After no increase or decrease in activity was observed for over 20 h, the catalyst was cooled down to below 20 °C in a flow of N_2 at a flow rate of 60 mL min^{-1} and then held under this flow for 5 h. After no ammonia formation was confirmed, the catalyst was heated at specific temperatures in a flow of N_2–H_2. The ammonia produced was trapped in 5 mM H_2SO_4 aqueous solution and the amount of NH_4^+ generated in the solution was estimated using an ion chromatograph (LC-2000 plus, Jasco) equipped with a thermal conductivity detector. The rate of ammonia formation was repeatedly measured more than 3 times after the ammonia formation rate remained constant for over 1 h. It was verified that the measured rate of ammonia formation had an error of less than 5%.

TOF was calculated from the ammonia formation rate and the number of surface zero-valent transition metal atoms (N_s) estimated on the basis of CO chemisorption values, assuming spherical metal particles. N_s for each tested catalysts was measured by CO-pulse chemisorption (BELCAT-A, BEL, Japan) at 50 °C using a He flow of 30 mL min^{-1} and pulses of 0.09 mL (9.88% CO in He).[7] Prior to these measurements, the catalyst after reaction was heated with flowing He (50 mL min^{-1}) at 300 °C for 1 h. The stoichiometry of the transition metal/CO was assumed to be 1. The transition metal particle size calculated from N_s is generally equal to that estimated by TEM observations.[29] However, the iron metal particle size of BaH_2-BaO/Fe was estimated from N_s to be larger than that (10–30 nm) expected from HAADF-STEM and EDX images (Fig. 2b) because N_s with the BaH_2-BaO layer on iron particles taken into account is necessarily smaller than the number of surface iron atoms calculated only from particle size.

$^{14}N_2$-$^{15}N_2$ isotropic exchange reaction

N_2 isotopic exchange was examined in a U-shaped glass reactor connected with a closed gas circulation system. A mixture of $^{15}N_2$ and $^{14}N_2$ (total pressure: 20.0 kPa, $^{15}N_2$:$^{14}N_2$ = 1:4) was adsorbed on the catalyst without circulation at the reaction temperature until adsorption/desorption was in equilibrium. The change in the composition of circulating gas was monitored by a quadrupole mass spectrometer (M-

101QA-TDM, Canon Anelva Co.). The m/z = 28, 29 and 30 signals were monitored as a function of time to follow the exchange.

Characterization. Powder X-ray diffraction (XRD; Miniflex600C, Rigaku) patterns were obtained using Cu Kα radiation. Nitrogen adsorption–desorption isotherms were measured at –196 °C with a surface-area analyzer (BELSORP-mini II, MicrotracBEL) to estimate the Brunauer-Emmett-Teller (BET) surface areas. The morphologies of the samples were observed using HAADF-STEM and EDX (JEM-ARM 200F, Jeol). H_2 and D_2-TPD were measured by heating (1 °C min^{-1}) a sample (ca. 100 mg) in a flow of Ar (30 mL min^{-1}), and the concentration of H_2 and D_2 was monitored with a mass spectrometer (BELMass, MicrotracBEL, Japan). FT-IR spectra were measured using a spectrometer (FT/IR-6100, Jasco) equipped with a mercury–cadmium–tellurium detector at a resolution of 4 cm^{-1}. Samples were pressed into self-supported disks. A disk was placed in a sealed and Ar-filled silica-glass cell equipped with NaCl windows to a closed gas-circulation system. The disk was heated under vacuum at 200 °C for 90 min. After the pretreatment, the disk was cooled to 25 °C under vacuum to obtain a background spectrum from the spectra of the N_2-adsorbed samples. Pure N_2 (99.99995%) was introduced into the system through a liquid-nitrogen trap. X-ray photoelectron spectroscopy (XPS; ESCA-3200, Shimadzu, Mg K*α*, 8 kV, 30 mA) was performed in conjunction with an Ar-filled glovebox, where the samples were moved to the ultra-high vacuum XPS apparatus through the Ar-filled glovebox without exposure to the ambient air. The binding energy was corrected with respect to the Au $4f_{7/2}$ peak of Au-deposited samples.

DFT computations. Total energies and structural relaxations of BaH_2 with/without surface H^- anion defects were estimated from density functional theory (DFT) computation based on VASP first-principles code. We adopted the Perdew–Burke–Ernzerhof (PBE) exchange-correlation functional in DFT. The convergence criteria of energy and force were, respectively, 0.5×10^{-4} eV and 1.0×10^{-1} eV nm^{-1} for all models. The core electrons were handled with the projector augmented wave (PAW) method. The k-point mesh was created to keep a single k-point per 1/4 (nm^{-1}) in the reciprocal space. In BaH_2, (0 0 1), (0 1 0), (1 0 0), (0 1 1), (1 0 1), (1 1 0), and (1 1 1) surface models were relaxed using DFT, and the (1 0 0) surface was the most stable surface for BaH_2 (0.37 J m^{-2}). A notable feature in the computation is that a vacuum region of 2 nm is maintained in the unit cell.

References

29. Larichev, Y. V. et al. XPS and TEM studies on the role of the support and alkali promoter in Ru/MgO and Ru-Cs^+/MgO catalysts for ammonia synthesis. *Appl. Surf. Sci.* **111**, 9427–9436 (2007).

30. Inoue, Y. et al. Direct activation of cobalt catalyst by $12CaO\cdot7Al_2O_3$ electride for ammonia synthesis. *ACS Catal.* **9**, 1670–1679 (2019).

Declarations

Acknowledgments

This work was supported by a fund from the Grants-in-Aid for Japan Society for the Promotion of Science (JSPS) Fellows and for Scientific Research from the Ministry of Education, Culture, Science, Sports, and Technology (MEXT) of Japan (17H06153).

Author contribution

M. Hattori designed the study, carried out catalyst synthesis, catalyst evaluation and mechanistic study and composed the manuscript. N.O. and H.K. performed catalyst evaluation and characterization. M. Hara supervised the study, planned the experiments and analyzed the data.

Figures

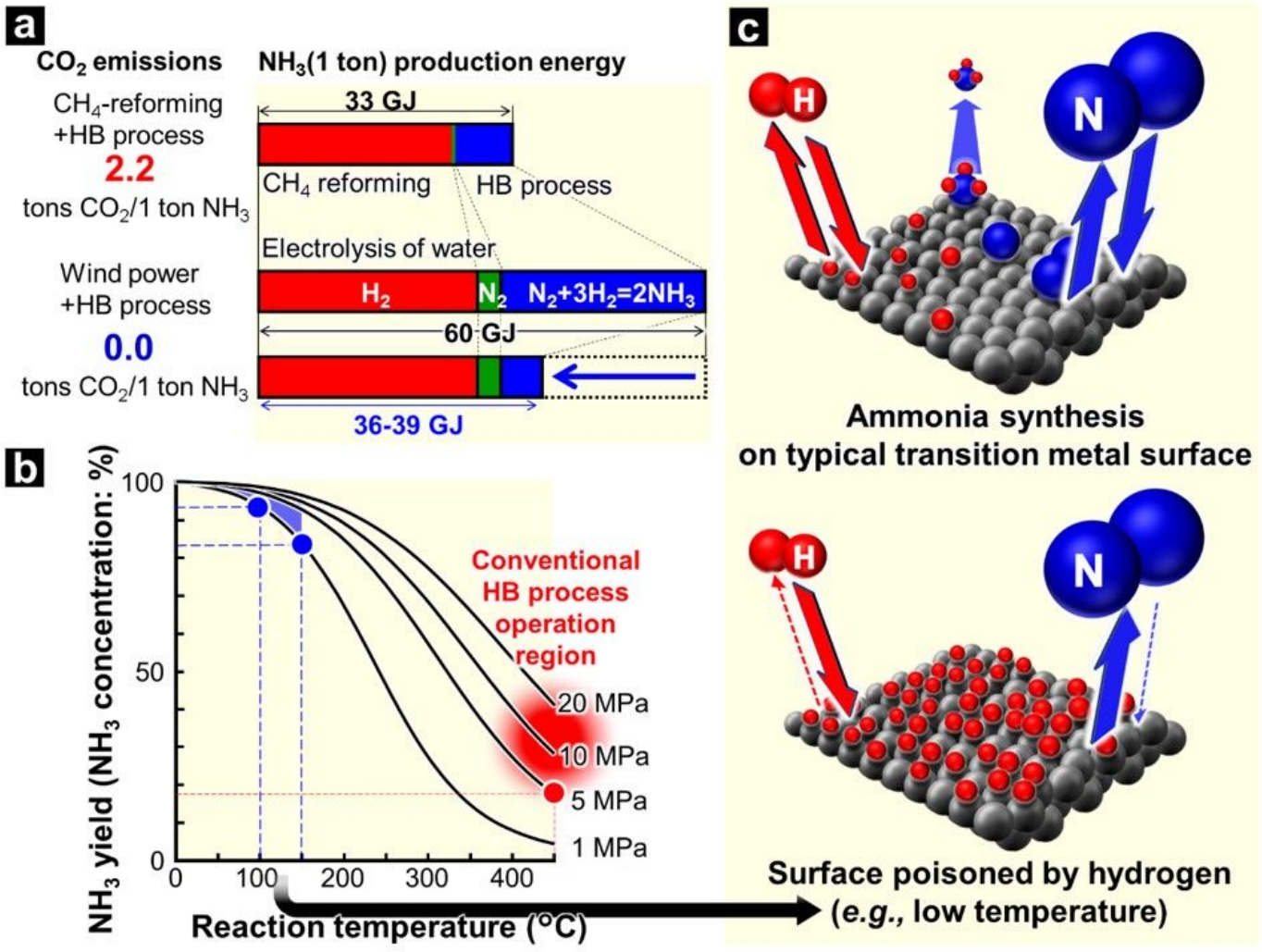

Figure 1

Ammonia synthesis. a, Ammonia production energies for the conventional HB process using H_2 produced by CH_4 reforming, and CO_2-free HB process using H_2 produced by water electrolysis based on wind power generation. The latter (60 GJ/NH_3 (1 ton)) is twice that of the former (33 GJ/NH_3 (1 ton)) because the HB

process is driven only by renewable electricity. By reducing the energy consumed for the HB process by 70 to 80%, the ammonia production energy for CO_2-free method can be decreased to 36–39 GJ/NH_3 (1 ton). **b,** Correlation of ammonia yield with temperature and pressure. For example, the maximum (theoretic) ammonia yield under 5 MPa at 450 °C, which is the operation temperature of the present HB process, is 0.86 MPa (= 5×0.17). On the other hand, ammonia synthesis under 1 MPa at 100 and 150 °C gives ammonia yields of 0.94 and 0.84 MPa, respectively. Therefore, 1/5 of the 5 MPa pressurization and 1/3–1/5 of the reaction temperature of 450 °C, *i.e.*, 20–30% of the energy consumption at 450 °C under 5 MPa, can produce as much ammonia or more than ammonia synthesis at 450 °C under 5 MPa; the energy consumed for the HB process can be reduced to 70 to 80%, as shown in Fig. 1a. **c**: Ammonia synthesis on a typical transition metal surface and adsorbed hydrogen atoms poisoning the transition metal surface.

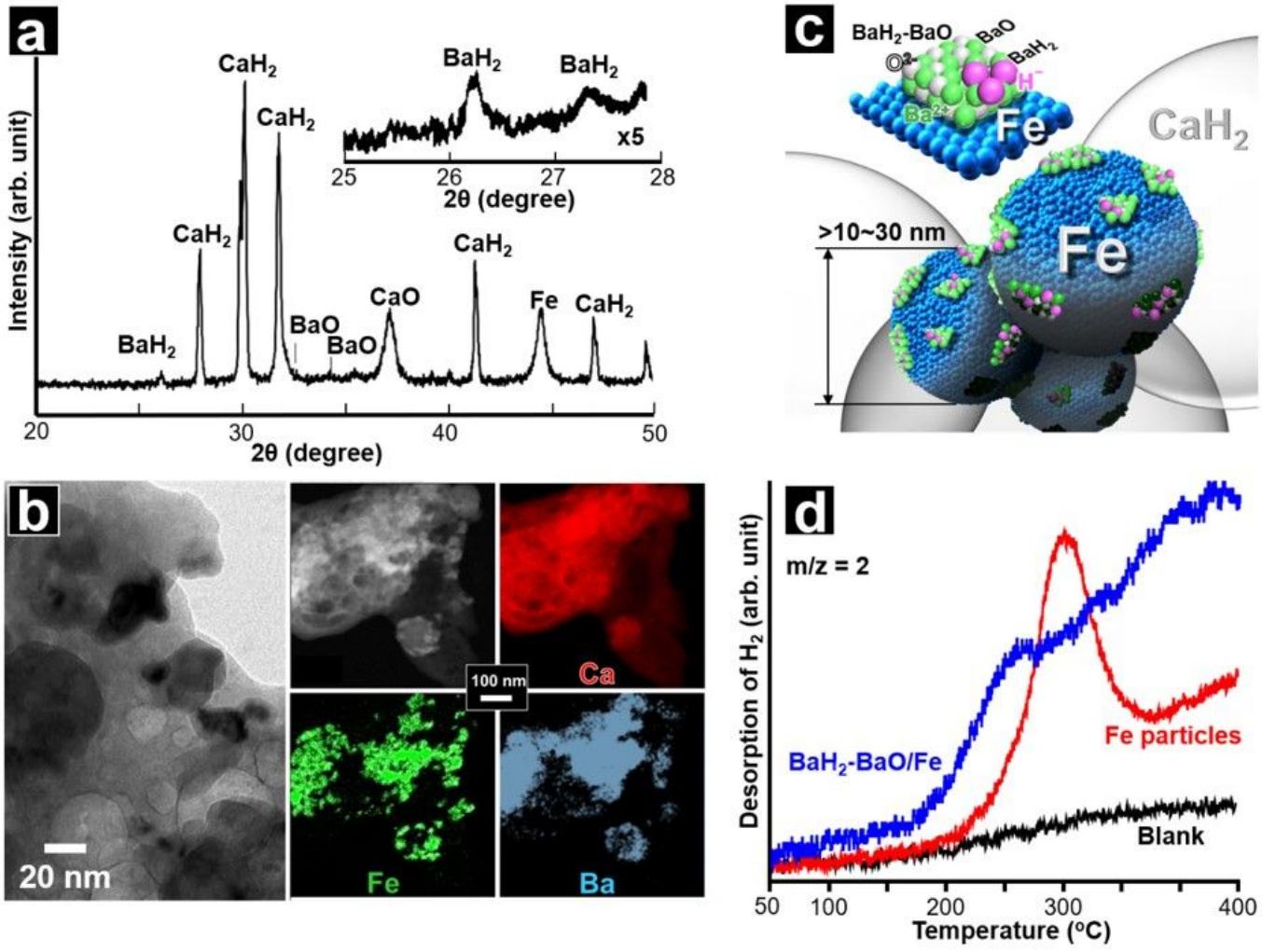

Figure 2

Structural and morphological data of BaH_2-BaO/Fe. a: Powder X-ray diffraction (XRD) pattern for BaH_2-BaO/Fe. **b**: High-angle annular dark field scanning transmission electron microscope (HAADF-STEM) and energy dispersive X-ray spectroscopy (EDX) images for BaH_2-BaO/Fe. **c**: Schematic structure of BaH_2-BaO/Fe. **d**: H_2 (m/z=2)-TPD profiles for metallic iron particles with and without BaH_2-BaO (BaH_2-BaO/Fe and Fe particles). Fe particles, metallic iron particles without BaO-BaH_2, was obtained by heating 0.019 g of α-Fe_2O_3 with 0.081 g of CaH_2 in a flow of H_2 (45 mL min^{-1}) at 300 °C for 2h. After ammonia synthesis at 300 °C for over 20 h, the catalyst was cooled down to room temperature and was then heated at a rate of 1 °C min^{-1}. Desorbed H_2 was detected with a quadrupole mass spectrometer.

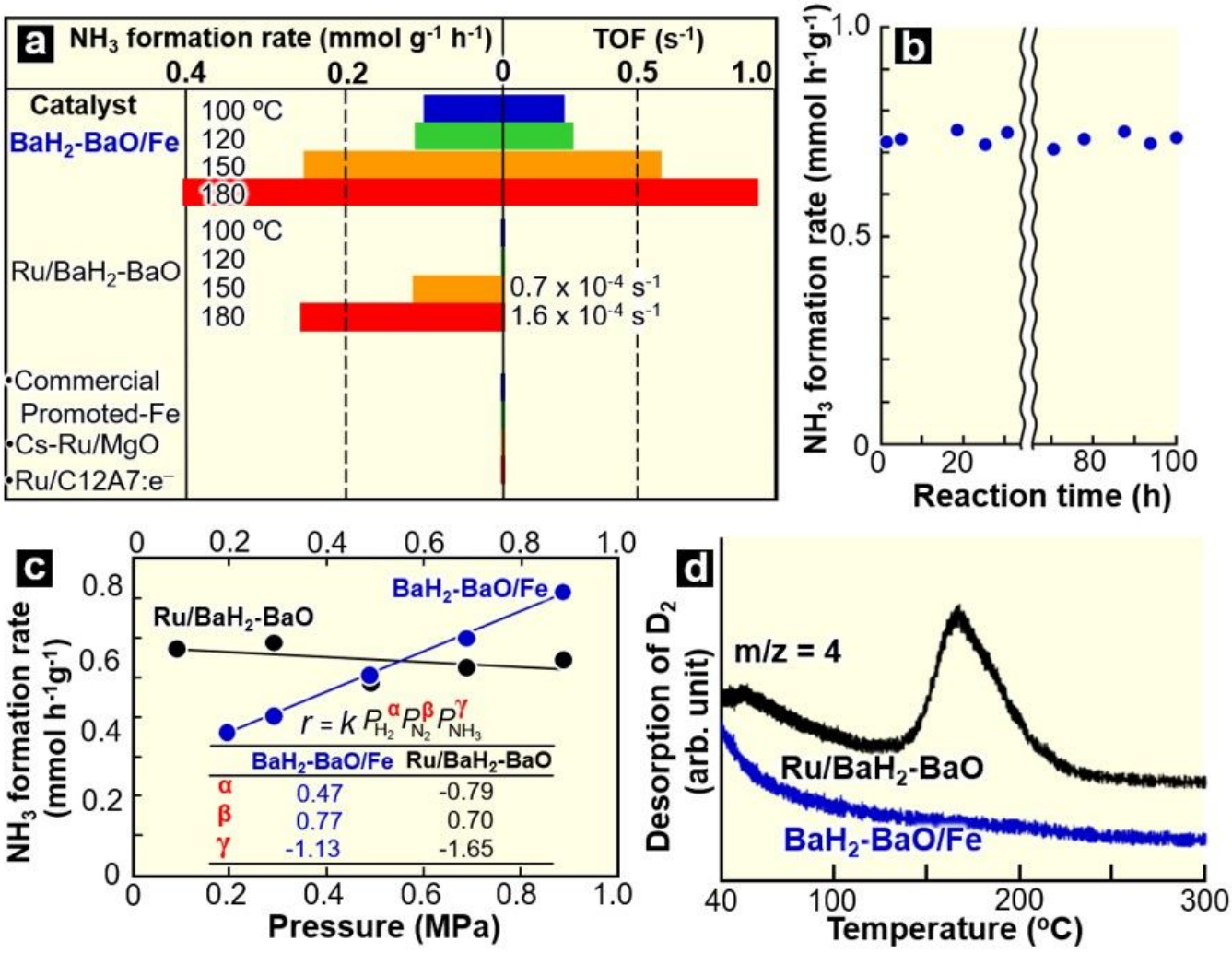

Figure 3

Catalytic performance and properties of BaH_2-BaO/Fe. a, Catalytic performance (ammonia formation rate and TOF) of the tested catalysts for ammonia synthesis at low temperatures. **b,** Time course of the ammonia formation rate on BaH_2-BaO/Fe at 200 °C. **c,** Correlation of the ammonia formation rate with pressure and the reaction orders for H_2, N_2 and NH_3 over BaH_2-BaO/Fe and Ru/BaH_2-BaO at 200 °C. **d,** D_2-

TPD (1 °C min^{-1}) for BaH_2-BaO/Fe and Ru/BaH_2-BaO in a flow of Ar. D adatoms were adsorbed onto the Fe and Ru surfaces in a flow of D_2 (15 mL min^{-1}, 30 min) at the room temperature.

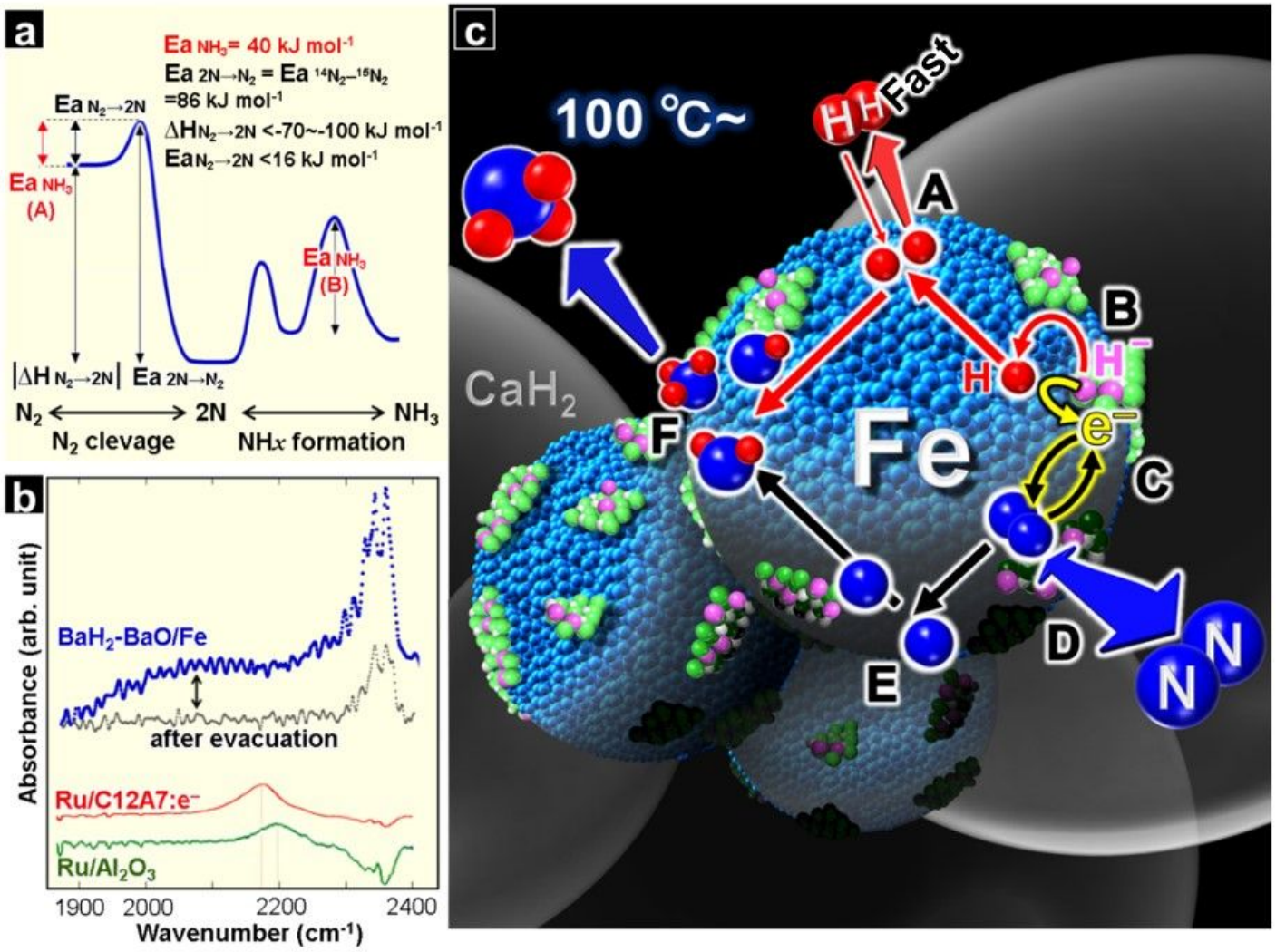

Figure 4

Thermodynamic and vibrational spectroscopic analyses, and schematic of the reaction mechanism for ammonia synthesis over BaH_2-BaO/Fe. a, Energy diagrams of ammonia formation over BaH_2-BaO/Fe. The activation energies for ammonia formation (Ea NH_3=40 kJ mol^{-1}) and $^{14}N_2$-$^{15}N_2$ isotropic exchange reaction ($^{14}N_2+{}^{15}N_2 \leftrightarrow 2{}^{14}N{}^{15}N$, Ea $^{14}N_2$–$^{15}N_2$=86 kJ mol^{-1}) were obtained from the Arrhenius plots for the reactions over the iron catalyst (Extended Data Figs. 2 and 3). Ea $^{14}N_2$–$^{15}N_2$ is equal to the activation energy of N_2 desorption (Ea 2N→N_2).[24-26] The dissociative adsorption heat of N_2 into N adatoms (ΔH N_2→2N) on a pure iron surface has been estimated to be -70 to -100 kJ mol^{-1}.[27] Electron donation from BaH_2-BaO to N adatoms stabilizes these atoms, which results in a larger dissociative adsorption heat on

BaH_2-BaO/Fe than that on pure Fe.[24,28] $\Delta H\ N_2 \rightarrow 2N$ would therefore be less than -70 to -100 kJ mol^{-1} ($|\Delta H\ N_2 \rightarrow 2N| \geq 70–100$ kJ mol^{-1}). **b,** FT-IR spectra for N_2-adsorbed BaH_2-BaO/Fe, Ru/C12A7:e^- and Ru/Al_2O_3. 10 kPa of N_2 at 25 °C. **c,** Schematic of the reaction mechanism for ammonia synthesis over BaH_2-BaO/Fe. The H_2 adsorption/desorption equilibrium is shifted toward H_2 desorption on metallic iron surfaces, even at low temperatures, which results in a low H adatom concentration (A). This induces some H^- anions in BaH_2-BaO to release H atoms as H_2 (B) and leaving electrons. The resulting hydride species with H^- defects and electrons can exhibit strong electron-donating power (C). The low H adatom concentration also contributes to provide sufficient adsorption sites for N_2 molecules (D). The strong electron donation from the hydride species to the antibonding π* orbitals of adsorbed N_2 facilitates the cleavage of adsorbed N_2 to N adatoms (D and E) and can decrease the activation energy for N_2 cleavage to less than those of the subsequent steps for N-Hn species formation; the latter step can be the rate-determining step of ammonia formation over BaH_2-BaO/Fe. The generated N adatoms react with H adatoms to form ammonia through the formation of N-Hn species (F).

Supplementary Files

This is a list of supplementary files associated with this preprint. Click to download.

- Extended220302.docx